ADVANCED MATERIALS

Supporting Information

for *Adv. Mater.*, DOI 10.1002/adma.202313252

Tailoring Single-Mode Random Lasing of Tin Halide Perovskites Integrated in a Vertical Cavity

Hamid Pashaei Adl, Jesús Sánchez-Díaz, Giovanni Vescio, Albert Cirera, Blas Garrido, Felipe Andres Vinocour Pacheco, Wiktor Żuraw, Łukasz Przypis, Senol Öz, Iván Mora-Seró, Juan P. Martínez-Pastor* and Isaac Suárez**

Tailoring single-mode random lasing of tin halide perovskites integrated in a vertical cavity

Hamid Pashaei Adl, Jesús Sánchez-Díaz, Giovanni Vescio, Albert Cirera, Blas Garrido, Felipe Andres Vinocour Pacheco, Wiktor Żuraw, Łukasz Przypis, Senol Öz, Iván Mora-Seró, Juan P. Martínez-Pastor* and Isaac Suárez **

S1. Design of the optical cavity.

In the optical cavity used in this work, the $FASnI_3$ film is deposited on the top of a commercial Distributed Bragg Reflector (DBR) and capped by a PMMA and an Au film. The device is expected to provide constructive interference of the lasing modes inside the semiconductor by matching the reflectivity spectra of the DBR and Au. For this purpose, the thicknesses of the different layers composing the device were chosen accordingly:

- DBR. A commercial DBR (63154, Edmund Optics) has been chosen as a bottom mirror (see Figure 1a). The mirror presents a maximum of reflectivity between 820 and 940 nm, where the $FASnI_3$ presents the PL band. Reflectivity of the mirror was experimentally characterized up to 900 nm (black line in Figure S1). This experimental curve can be reproduced with a transfer matrix algorithm (red line in Figure S1) by assuming that the mirror is composed by alternating 12 periods of SiO_2/TiO_2 layers with a thickness of one quarter the operation wavelength: $\lambda/4n$, where n is the refractive index of the corresponding material and $\lambda = 880$ nm, the central wavelength. The drop on the experimental reflectivity is ascribed to the limit of the detector system.

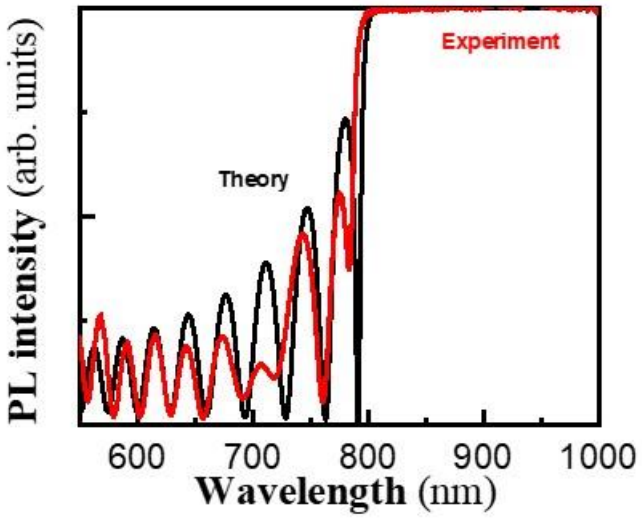

Figure S1. Characterization of the commercial mirrors and fitting with a transfer matrix method.

- A $FASnI_3$ film is deposited on the top of the mirror to act as the active media inside the cavity. At these conditions, the thickness of the film was fixed to be close to half the operation wavelength $d_1=\lambda/2n \approx 200$ nm, where $\lambda = 880$ nm and n is the refractive index of $FASnI_3$.
- PMMA. The PMMA not only protects the LFP against air moisture, but also allows controlling the spectral position of the cavity mode. In this way, this thickness was carefully modified in twelve different samples to tune the resonant mode between 800 and 900 nm. In particular, $d_2=250$ nm provides the resonance at 890 nm (ASE band).
- Au. The metal will act as a top reflector for the emitted light. A $d_3=30$ nm thick metal was chosen to provide a good compromise between a high reflectivity (obtained with thicker metals) and enough transmittance for the emitted light (obtained with thin metals).

Table S1. Summary of samples

DBR	**M0(eV)**	**P_{th}** ($\mu J/cm^2$)	**ASE** (eV)	**RL** (eV)
1	1.35-1.36	383-578	1.38-1.39	1.39-1.40
2	1.42-1.45	13-66	1.40-1.41	1.40-1.41
3	1.54	139-148	1.41	no
4	-	132-196	1.39-1.40	no
5	-	132-179	1.38-1.40	no
6	1.47-1.48	69	1.40-1.41	no
7	1.45-1.55	126-156	1.38-1.39	no
8	1.42-1.47	10-88	1.38-1.39	1.39-1.41
9	1.37-1.39	200-500	1.37-1.38	no
10	1.428	no	1.37-1.38	no
11	1.42-1.49	29-84	1.37-1.40	1.39-1.41
12	1.50	161-166	1.37-1.38	no

S2. Experimental reflectivity.

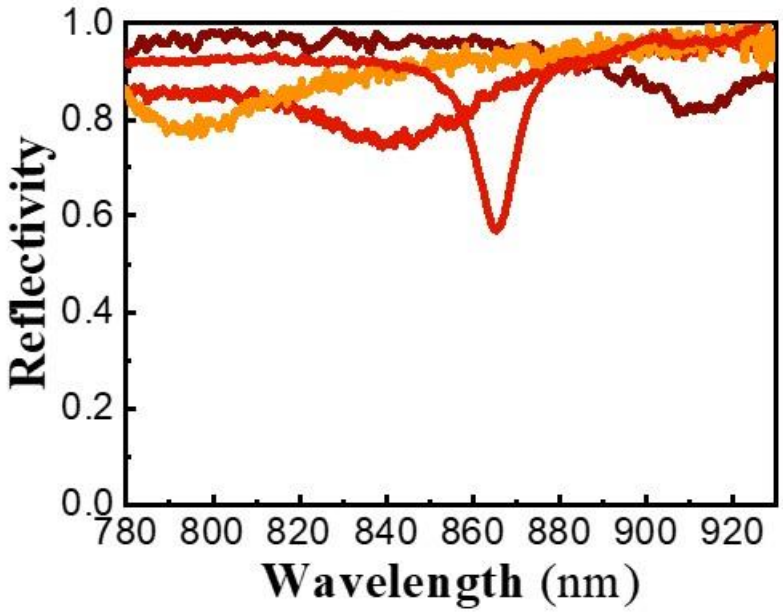

Figure S2. Experimental reflectivity in several samples with different d_1.

S3. PL spectra in above threshold in linear scale.

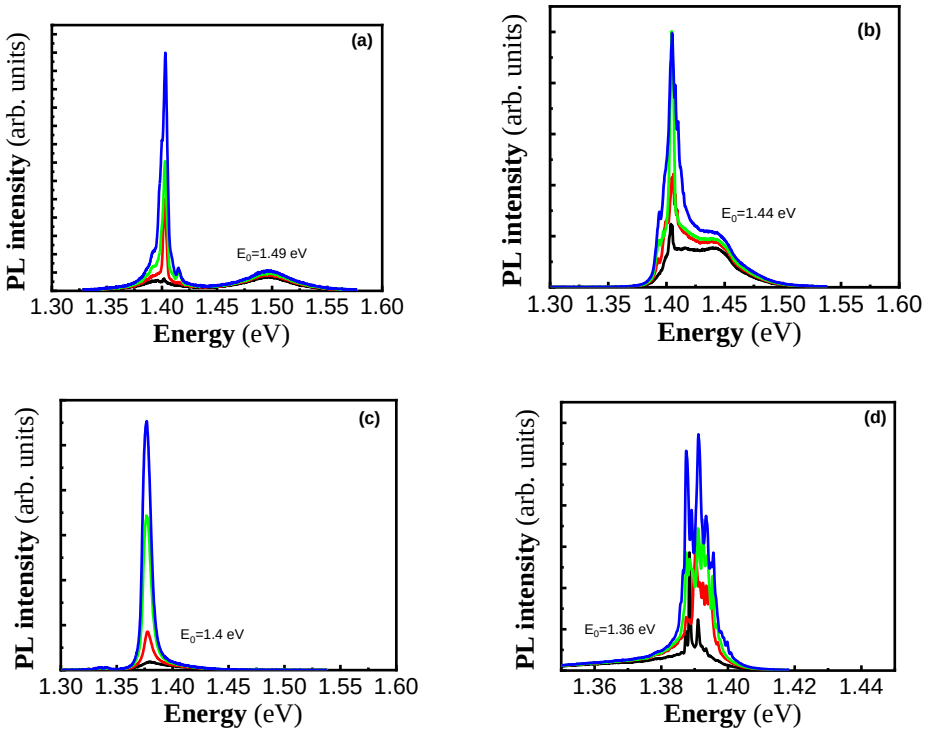

Figure S3. PL spectra above threshold in linear scale. (a) E_0=1.49 eV, (b) E_0=1.44 eV, (c) E_0=1.40 eV and (d) E_0=1.36 eV,

S4. Rate equation model.

The generation of carriers (n) and photons (S) was fitted by the standard rate equation model for lasers considering the generation of three different flows of photons accounting for the mode of the cavity (M0) and the ASE/RL band (ASE).

$$\frac{\partial n}{\partial t} = G - A_{nr} \cdot n - A_r \cdot n - \sum_i \left(\Gamma_i \cdot \sigma_i \cdot \frac{c}{n_{eff,i}} \cdot (n - N_i) \cdot S_i \right) \quad (1)$$

$$\frac{dS_i}{dt} = \left(\Gamma_i \cdot \sigma_i \cdot \frac{c}{n_{eff,i}} \cdot (n - N_i) - \frac{1}{\tau_{c,i}} \right) \cdot S_i + A_r \cdot \beta_i \cdot n \quad (2)$$

where the subindex i refers to M0 and ASE, A_r is the radiative recombination rate (inverse of the recombination time), A_{nr} is the nonradiative recombination rate, σ the gain cross section, N_0 the transparence carrier density, n_{eff} the effective refractive index of the mode at 890 nm, Γ the confinement of the mode at 890 nm in the FASI film, β the spontaneous

emission factor, *S* the photon density, c the speed of light, τ_c the loss of photons inside the cavity, and *G* is the photogeneration of electron-hole pairs:

$$G = \frac{P}{A \cdot h\nu} \cdot \alpha_p \quad (3)$$

where *P* is the excitation peak power, α the absorption coefficient at the excitation wavelength, *A* the area of excitation and $h\nu$ the energy of the pump photon at 532 nm (2.33 eV). Equations (1-2) include the optical gain in the system for each mode that is given by:

$$g_i = \Gamma_i \cdot \sigma_i \cdot \left(n - N_{0,i}\right) \quad (4)$$

Equations (1-4) nicely fit the experimental results of the PL shown in the Fig. 2c by using A_{ri}=0.7, A_{nr}=0 and the parameters listed in the table S2. The transparent carrier densities, $N_{0,i,}$ depend on the emission energy (wavelength) and cannot be directly obtained from the excitation fluence at threshold, P_{th}. Then, $N_{0,i}$ is set as the theoretical transparency obtained for $FASnI_3$ ($1.3 \cdot 10^{18}$ cm^{-3}) at the PL wavelength, and corrected for higher energies by the absorption spectra. Besides, τ_c is estimated by the linewidth above threshold (≈10-100 meV) to be ≈0.1 ps for all emission energies. At these conditions, the β and Γ·σ are obtained from the first fitting of the curves. The parameter β indicates the portion of the emission which is coupled to a mode and has an important impact in the correct fitting of the ASE curve. Interestingly, β_{ASE} increases with E_0 in spite of the larger spectral shift. This is because the longitudinal (M0) and guided (G) modes are two mechanisms competing for the emitted PL. For E_0<X, M0 experiences smaller gain and most of the emitted light propagates along the $FASnI_3$ plane leading to ASE. Nevertheless, for E_0>X, there is an efficient cavity-exciton coupling that results on a more equitable distribution of PL between the M0 and G modes and a higher β. On the other hand, β_{M0} has little influence on the fitting due to the lower intensity of S_{M0} above threshold. The parameter Γ·σ comprises the confinement factor of the mode at the emission wavelength and the emission cross section extracted from the top of the cavity. The confinement of the resonant mode is set to Γ_{M0}=0.1 according to the simulations of the electric field in the cavity, while Γ_{ASE} and Γ_{M1} strongly depends on the E_0-E_{PL} shift: for E_0-E_{PL}=0 reaches Γ_{ASE}= Γ_{M1} =0.1 and it is reduced to 10^{-3}-10^{-4} if the overlap is weaker. In this way, fixing $\Gamma \cdot \sigma_{M0}=10^{-20}$ cm^2, the fitting indicates the highest $\Gamma \cdot \sigma_{ASE}=0.8 \cdot 10^{-18}$ cm^2 for E_0=1.40 eV where M0 overlaps the PL band. Considering that Γ_{ASE}=0.1 for this mode position, the

top emission cross section σ_{ASE}~10^{-16} cm^2 , which is two-fold smaller than that deduced for in-plane propagation. Finally, the carrier density, N, can be plotted as a function of the excitation fluence, see Fig. S4a, to extract the density of carriers to estimate the optical gain in the different samples, see Fig. S4b.

Table S2. Fitting parameters used in Fig. 2c.

E_0(eV)	N_0 (10^{18} cm^{-3})		β		Γ·σ ($10^{-20}cm^2$)		τ_c (ps)	
	M0	ASE	M0	ASE	M0	ASE	M0	ASE
1.54	9.8	1.3	0.05	0.2	1	2000	0.1	0.1
1.49	6.5	1.3	0.05	0.15	1	3000	0.1	0.1
1.44	4	1.3	0.05	0.14	1	4500	0.1	0.1
1.4	1.3	1.3	0.05	0.02	1	8000	0.1	0.1
1.35	1.3	1.3	0.05	0.01	1	300	0.1	0.1

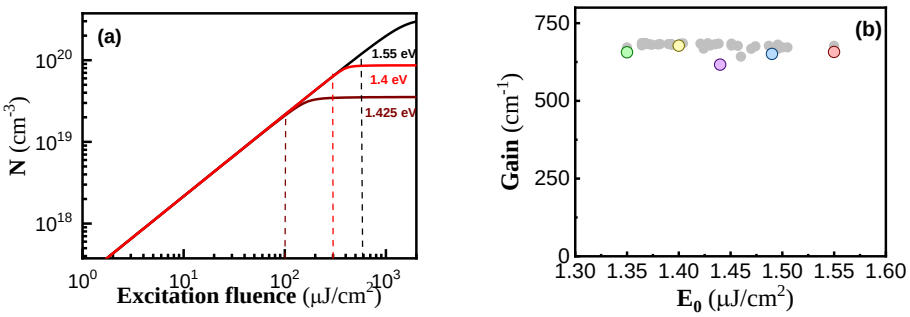

Figure S4. (a) Carrier density as a function of the excitation fluence. (b) Optical gain extracted in the different samples. Color symbols represent the data shown in Fig. 2.

S5. Estimation of the PL enhancement and Purcell factor.

Under the experimental conditions carried out here, the determination of the Purcell factor (F_p) with the recombination time is strongly limited by the nonradiative channels. In this way, Fp, is estimated by the overlap of the mode and the PL band (see ref. 37 of the manuscript). Besides, the PL enhancement (PL_{enh}) in each sample is estimated here by calculating the normalized integrated intensity of the mode below threshold and dividing this value with the integration of the normalized PL band at the same spectral region.

$$PL_{enhP} = \frac{\int_{E0}^{E1} M(E)dE}{\int_{E0}^{E1} PL(E)dE} \quad (5)$$

where M(E) refers the spectral distribution of the mode below threshold, PL the photoluminescence measured by back-scattering, and the integration limits E0 and E1 are

fixed to sweep the linewidth of the mode. At these conditions, we deduce the relative dependence of PF with respect the mode position illustrated in Figure S5.

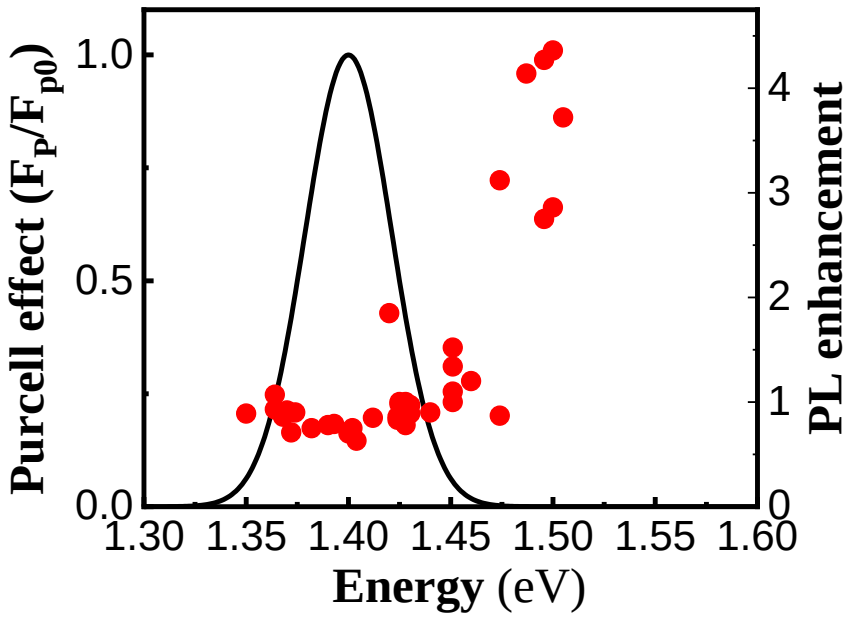

Figure S5. Solid line and left axis. Purcell effect in relative units. Symbols and right axis. PL enhancement due to M0 coupling, as estimated in each sample as a function of the mode position.

S6. RL loops.

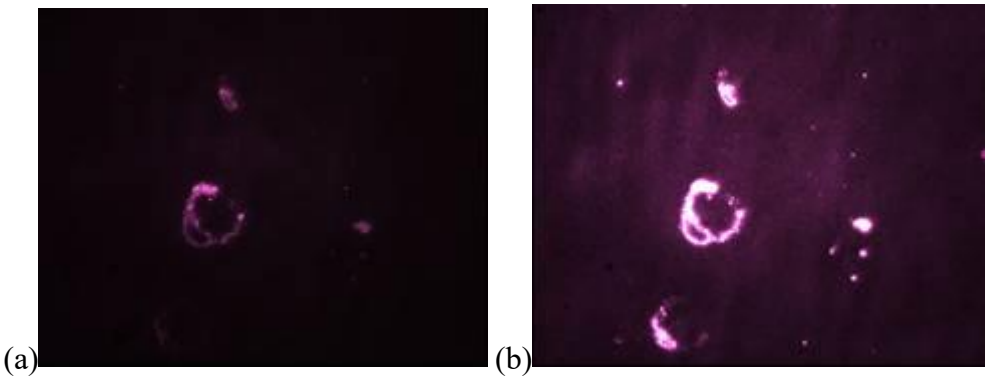

Figure S6. Photograph of RL loops at (a) threshold (b) maximum excitation fluence. Size of the image is around 500 μm.

S7. Mode stability.

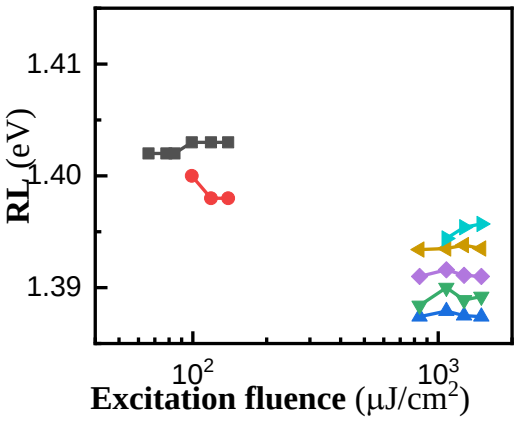

Figure S7. Evolution of RL modes with the excitation fluence.

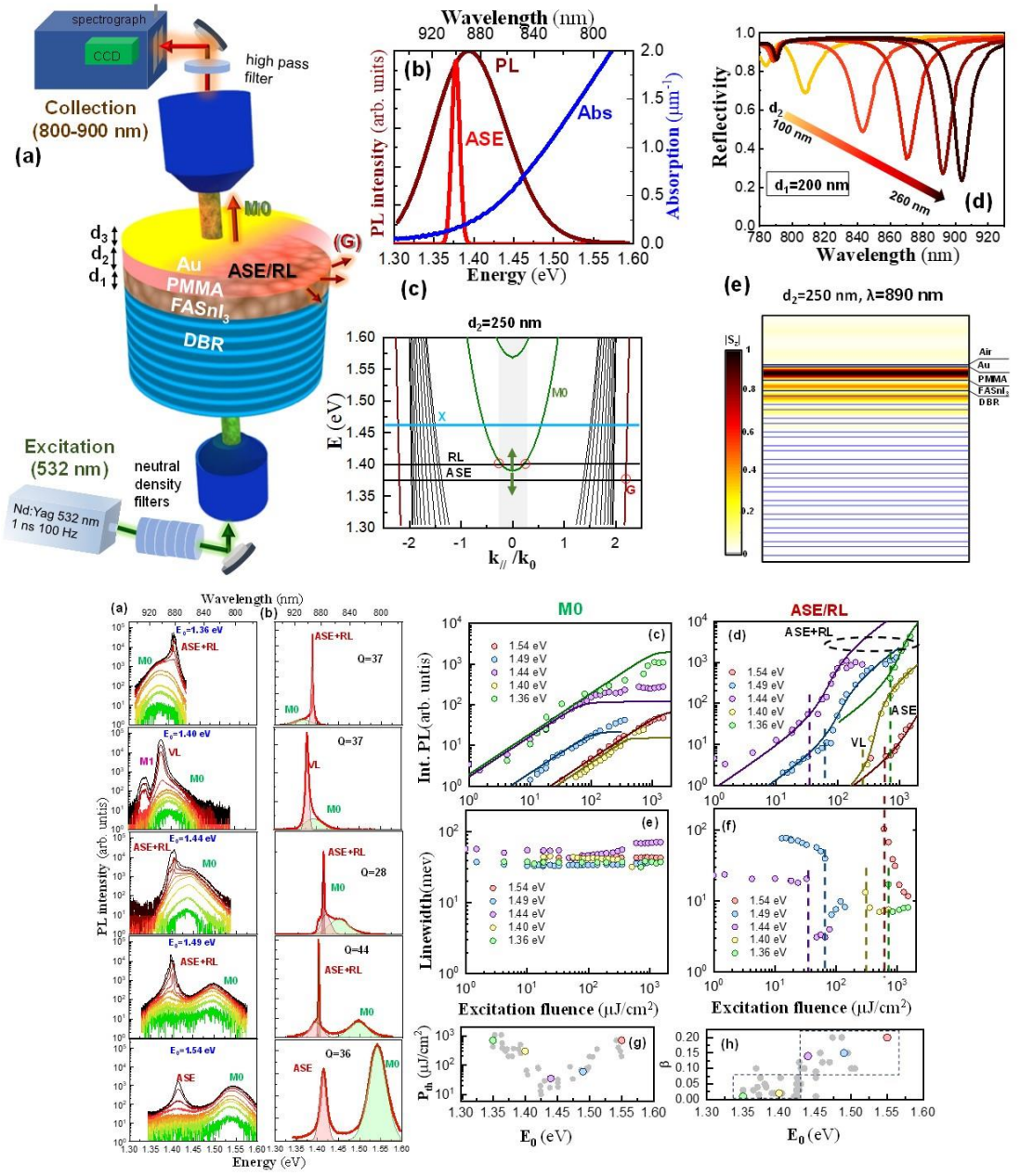
spectrograph
CCD
high pass filter
Collection (800-900 nm)
(a)
M0
d3
d2
d1
Au
PMMA
FASnI3
DBR
ASE/RL
(G)
Excitation (532 nm)
neutral density filters
Nd:Yag 532 nm 1 ns 100 Hz
Wavelength (nm)
920 880 840 800
(b)
PL
ASE
Abs
PL intensity (arb. units)
Absorption (μm-1)
Energy (eV)
(c)
d2=250 nm
E (eV)
X
M0
RL
ASE
G
k// /k0
Reflectivity
d2
100 nm
260 nm
d1=200 nm
(d)
Wavelength (nm)
(e)
d2=250 nm, λ=890 nm
|S2|
Air
Au
PMMA
FASnI3
DBR
(a)
(b)
Wavelength (nm)
E0=1.36 eV
ASE+RL
M0
Q=37
E0=1.40 eV
M1
VL
E0=1.44 eV
Q=28
E0=1.49 eV
Q=44
E0=1.54 eV
ASE
Q=36
PL intensity (arb. units)
Energy (eV)
M0
ASE/RL
(c)
(d)
1.54 eV
1.49 eV
1.44 eV
1.40 eV
1.36 eV
Int. PL(arb. units)
ASE+RL
ASE
VL
(e)
(f)
Linewidth(mev)
Excitation fluence (μJ/cm2)
(g)
(h)
Pth (μJ/cm2)
β
E0 (eV)

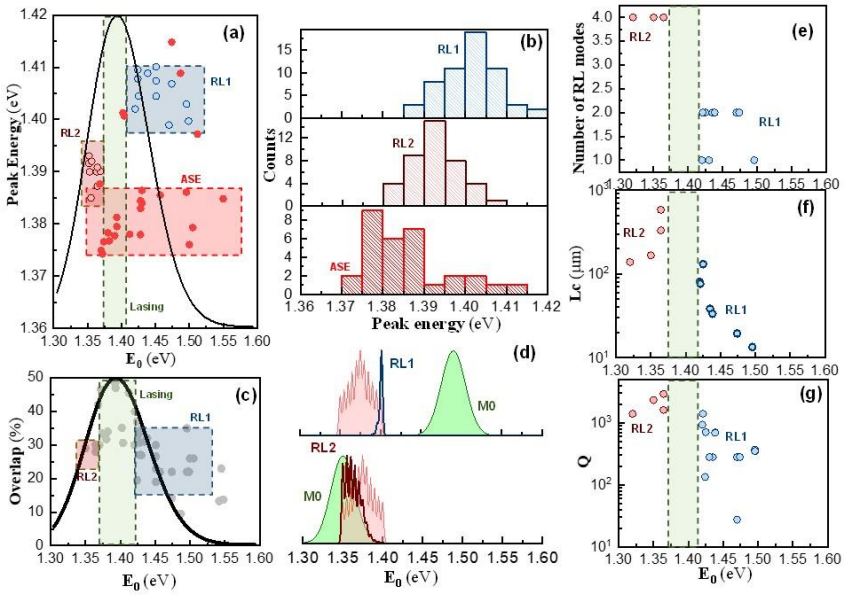
(a)
Peak Energy (eV)
RL1
RL2
ASE
Lasing
E0 (eV)
(b)
Counts
RL1
RL2
ASE
Peak energy (eV)
(c)
Overlap (%)
Lasing
RL1
RL2
E0 (eV)
(d)
RL1
M0
RL2
M0
E0 (eV)
(e)
Number of RL modes
RL2
RL1
(f)
Lc (μm)
RL2
RL1
(g)
Q
RL2
RL1
E0 (eV)

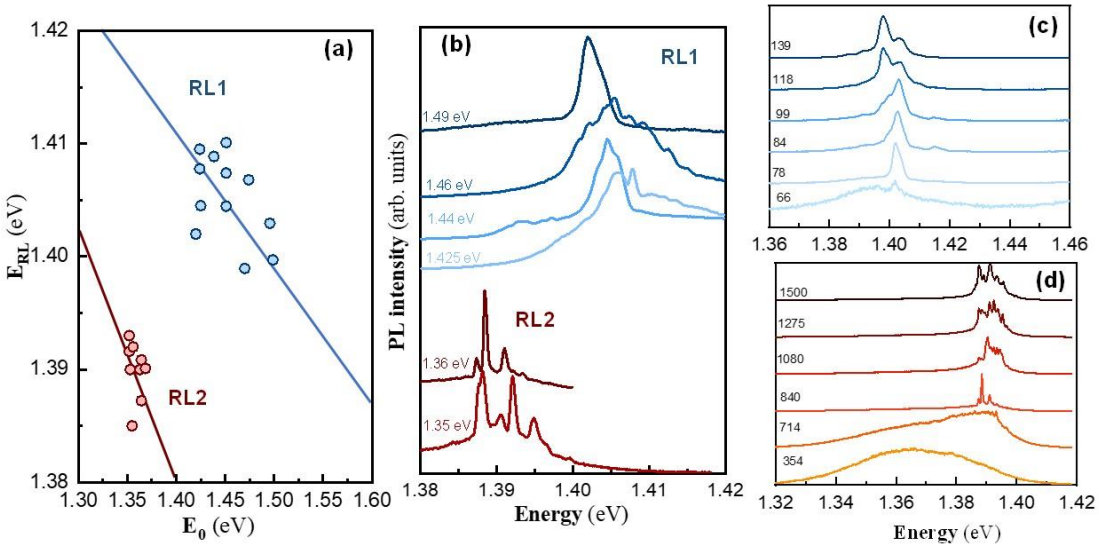
(a)
RL1
RL2
E_RL (eV)
E0 (eV)
(b)
RL1
1.49 eV
1.46 eV
1.44 eV
1.425 eV
RL2
1.36 eV
1.35 eV
PL intensity (arb. units)
Energy (eV)
(c)
139
118
99
84
78
66
(d)
1500
1275
1080
840
714
354
Energy (eV)

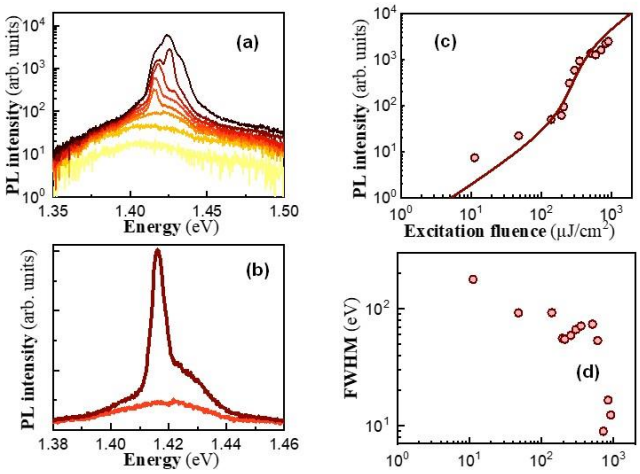
(a)
PL intensity (arb. units)
Energy (eV)
(b)
PL intensity (arb. units)
Energy (eV)
(c)
PL intensity (arb. units)
Excitation fluence (μJ/cm²)
(d)
FWHM (eV)